Elsevier Editorial System(tm) for Materials Science and Engineering C
Manuscript Draft

Manuscript Number:

Title: Fabrication and in vitro characterization of nanoporous calcium phosphates with controlled porosity and composition

Article Type: Research Paper

Keywords: calcium phosphate; nanoparticle; assembly; nanopore; osteoblast

Corresponding Author: Dr. Masahiro Okada, Ph.D.

Corresponding Author's Institution: Osaka Dental University

First Author: Keiko Fujiwara

Order of Authors: Keiko Fujiwara; Masahiro Okada, Ph.D.; Shoji Takeda; Naoyuki Matsumoto

Abstract: Hypothesis: Biphasic calcium phosphate (BCP) consisting of hydroxyapatite (HAp) and β-tricalcium phosphate (β-TCP) is usually prepared by thermal decomposition of calcium-deficient HAp (CDHAp), the calcium deficiency and morphology of which are usually difficult to manipulate in parallel. It is likely easier to control the composition and morphology of BCP by using only a certain type of CDHAp nanoparticle as a building block and by adjusting the calcium deficiency (Ca/P ratio) of the nanoparticle-assembled (or nanoporous) CDHAp prepared by drying a CDHAp aqueous dispersion that contains water-soluble Ca or PO4 salts.
Experiments: An aqueous dispersion of CDHAp (Ca/P molar ratio, 1.61) nanoparticles was prepared via a wet chemical process. After Ca(NO3)2 or (NH4)2HPO4 was dissolved to adjust the Ca/P ratio (1.50-1.67) in the dispersion, a nanoparticle-assembled plate was prepared by drying the dispersion on an oil substrate, followed by thermal treatment at 1000°C. In vitro tests were conducted with preosteoblast cells.
Findings: The composition of BCP could be predictably controlled by adjusting the Ca/P ratio in the dispersion. The Ca/P ratio did not significantly vary the grain size (210-300 nm) and the pore size (140-170 nm) of the composition-controlled BCP. In vitro tests exhibited preferred cell adhesion on nanoporous BCPs compared with densely-sintered pure HAp, and cell differentiation was promoted on the nanoporous pure HAp.

Graphical abstract

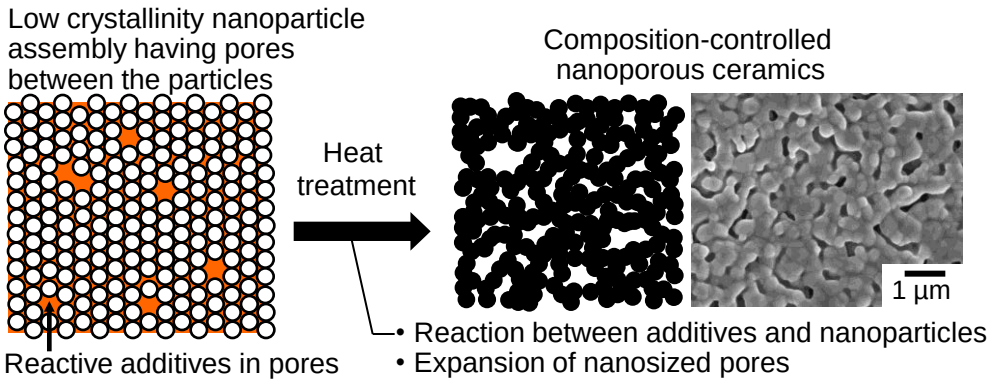

Research highlights (maximum 85 characters, including spaces, per bullet point)

► Nanoporous biphasic calcium phosphates (BCPs) were fabricated.
► Novel approach to control compositions of BCPs was shown.
► Morphologies of BCPs with varying composition were similar.
► This method requires no pore generation agents such as micelles and porogens.

Fabrication and in vitro characterization of nanoporous calcium phosphateswith controlled porosity and composition

Keiko Fujiwara[1,*], Masahiro Okada[2,*],Shoji Takeda[2], Naoyuki Matsumoto[1]

[1]Graduate School of Dentistry, Department of Orthodontics, Osaka Dental University, 8-1 Kuzuha-Hanazono, Hirakata, Osaka 573-1121, Japan

[2]Department of Biomaterials, Osaka Dental University, 8-1 Kuzuha-Hanazono, Hirakata, Osaka 573-1121, Japan

*Corresponding authors:

K. Fujiwara: keiko.reboot@gmail.com (Tel: +81-72-864-3078)

M. Okada: okada-m@cc.osaka-dent.ac.jp (Tel: +81-72-864-3111)

Abstract

Hypothesis: Biphasic calcium phosphate (BCP) consisting of hydroxyapatite (HAp) and β-tricalcium phosphate (β-TCP) is usually prepared by thermal decomposition of calcium-deficient HAp (CDHAp), the calcium deficiency and morphology of which areusually difficult to manipulatein parallel. It is likely easier to control the composition and morphology of BCP by using only a certain type of CDHAp nanoparticle as a building block and by adjustingthe calcium deficiency (Ca/P ratio)of the nanoparticle-assembled (or nanoporous) CDHAp prepared by drying a CDHAp aqueous dispersionthat containswater-soluble Ca or PO_4 salts.

Experiments: An aqueous dispersion ofCDHAp (Ca/P molar ratio, 1.61) nanoparticleswas prepared via a wet chemical process. After $Ca(NO_3)_2$ or $(NH_4)_2HPO_4$ was dissolved to adjust the Ca/P ratio (1.50–1.67) in the dispersion, a nanoparticle-assembled plate was prepared by drying the dispersion on an oil substrate, followed by thermal treatmentat 1000°C. In vitro tests were conducted with preosteoblast cells.

Findings: The composition of BCPcould be predictably controlled byadjustingthe Ca/P ratio in the dispersion. TheCa/P ratio did not significantly vary the grain size (210–300 nm) and the pore size (140–170 nm)of the composition-controlled BCP.In vitro testsexhibited preferred cell adhesion on nanoporous BCPs compared with densely-sintered pure HAp, and cell differentiation was promoted on the nanoporous pure HAp.

Keywords: calcium phosphate; nanoparticle; assembly; nanopore; osteoblast

1. Introduction

Calcium phosphate-based bioceramics have been shown to be attractive materials for biological applications [1–3]. Among these bioceramics, particular attention has been given to hydroxyapatite (HAp: $Ca_{10}(PO_4)_6(OH)_2$; Ca/P molar ratio, 1.67) because of its bioactivity, and to β-tricalcium phosphate (β-TCP: $Ca_3(PO_4)_2$; Ca/P molar ratio, 1.50)because of its resorbability [4]. To achieve optimum resorbability, biphasic calcium phosphate (BCP: a mixture of HA and β-TCP) was developed [5–9]. The first studies on BCP reported by LeGeros*et al.* demonstrated that the bioactivity of BCP could be controlled by manipulating the composition (HA/β-TCP ratio) of BCP [7,8].

The most common methodto prepare BCP is the thermal decomposition of nonstoichiometric calcium-deficient HAp (CDHAp; $Ca_{10-x}(HPO_4)_x(PO_4)_{6-x}(OH)_{2-x}$; $0 < x < 1$) at temperatures above 700°C [10]. The composition of BCP obtained after thermal treatment depends on the calciumdeficiency of CDHAp and the treatment temperature [9,10]. Although CDHAp is usually prepared via wet chemical processes by manipulating reaction conditions (such as initial Ca/P value, pH, and temperature), predicting the calcium deficiency (Ca/P ratio) is difficult and the particle morphologies (i.e., size and shape) also vary depending on the reaction conditions [9–12].Recently, Descamps*et al.*fabricated denselysintered BCPs with well-controlled compositions and with almost the same morphologies (grain size, 0.67–0.79 μm) by means of hot isostatic pressing (HIP) sintering ofCDHAp prepared by wet chemical processes under fine-tuned conditions [13].

Other methods to prepare BCP include solid-state reactions of mixtures of $CaHPO_4 \cdot 2H_2O/CaCO_3$ [14,15], $Ca_3(PO_4)_2/Ca(OH)_2$ [16], and $Ca(H_2PO_4)_2 \cdot H_2O/CaCO_3$[17,18]. The sintering of a mixture of pure (stoichiometric) HAp

powders and pureβ-TCP powders has been developed to easily control the composition of the resultant BCP [19,20]. However, the above-mentioned solid-state reactions and sintering (i.e., mixing of different sized particles)are not recommended for the production of BCP with reproducible compositions and homogeneous crystal distributions [1].

Recently, nanostructured calcium phosphate ceramics have attracted interest because of their improved bioactivity compared with that of conventional ceramics [21–25]. For example, Webster *et al.* showed enhanced osteoclast-like cell adhesion and function on HAp ceramic surfaces that had nanometer-sized surface topographies [21, 22]. Sun *et al.* reported that nanophase HAp can more effectively promote the proliferation and osteogenic differentiation of periodontal ligament cells compared with dense HAp [23].

We have developed a facile colloidal process for preparing nanoparticle-assembled CDHAp involving thedrying of an aqueous dispersion of low-crystallinity CDHAp nanoparticles on an oil (flowable) substrate without template/binder molecules or high-temperature/pressure treatments [26]. In our previous study, we investigated thermally induced changes of nanoparticle-assembled CDHAp, and a nanoporous BCP (with pore sizesthat varied from 65 to 250 nm) was obtained after thermal treatment above 800°C [27]. We hypothesized that it would be possible to prepare composition-controlled nanoporous BCPs by a thermal treatment of nanoparticle-assembled CDHAp whose Ca/P ratios were manipulated during nanoparticle assembly. That is, by using only a type of CDHAp nanoparticle as a building block and by adjusting theCa/P ratio by adding water-soluble Ca or PO_4 salts to the aqueous dispersion of CDHAp nanoparticles, the Ca or PO_4 salts are expected to be homogeneously distributed in the nanopores of nanoparticle-assembled CDHAp (prepared by drying the aqueous dispersion of the CDHAp nanoparticles after

water-soluble Ca or PO_4 salts were homogeneously dissolved).Hence, the homogeneous reaction between CDHAp nanoparticles and the Ca or PO_4 salts could be achieved, andthe resultant composition-controlled nanoporous BCPs could have the same surface morphologies (i.e., grain and pore sizes) to each other.

The objective of this study is to investigate the effects of water-soluble Ca or PO_4 salts added to the nanoparticle-assembled CDHAp on the formation of nanoporous BCP after thermal treatment. Here, particular attention is given to crystal phase, surface morphologies (grain size and surface porosity), and open pore size (and its distribution), which were investigated using X-ray diffraction (XRD), scanning electron microscopy (SEM), and mercury intrusion porosimetry, respectively. Cell adhesion and differentiation behaviors on nanoporous BCPs were compared to investigate the influence of the composition of BCP withsimilar surface nanoporous structures.

2. Experimental Section

2.1. Materials

Unless stated otherwise, all materials were reagent gradeand used as received from Wako Pure Chemical Industries, Ltd., Osaka, Japan. Milli-Q water (Millipore Corp., Bedford, MA) with a specific resistance of $18.2 \times 10^6 \Omega \cdot cm$ was used.

2.2. Low crystallinity CDHAp nanoparticles

An aqueous solution of $Ca(NO_3)_2$ (42 mM, 800 mL), whose pH was adjusted to 12.0 via the addition of 28% ammonia solution, was poured into a 1-L reactor equipped with a magnetic stirrer and an inlet for nitrogen gas. After the reactor temperature was equilibrated

to room temperature, an aqueous solution of $(NH_4)_2HPO_4$ (100 mM, 200 mL) was added to the reactor within 5 s, and the resultant mixture was stirred for another 24 h. The resulting product was then centrifugally washed five times with Milli-Q water, following whichit was redispersed in water (solid content, 2.0 wt.%).

The nanoparticles were observed using SEM (S-4800; Hitachi High Technologies Corp., Tokyo, Japan)at 5 kV after the samples were dried on an aluminum stub at room temperature and sputter-coated with Pt–Pd to minimize sample-charging problems. The number-averaged particle size (N = 50) was determined from SEM photographs.

The Ca/P molar ratio of the nanoparticles was measured with an inductively coupled plasma-atomic emission spectrometer (ICP-AES: SPS4000; Seiko Instrument Inc., Chiba, Japan).Calcium and phosphorus standard solutions for ICP-AES were purchased from Kanto Chemical Co., Inc., Tokyo, Japan.

2.3. Nanoporous calcium phosphates

First, an amount of $Ca(NO_3)_2{\bullet}4H_2O$ (0.05–0.10 g vs. 1 g of nanoparticles) or $(NH_4)_2HPO_4$ (0.025–0.05 g vs. 1 g of nanoparticles) was dissolved in an aqueous dispersion of low crystallinity CDHAp (Ca/P molar ratio, 1.61), and the Ca/P molar ratio in the dispersion was adjusted to be 1.50–1.67. After the dispersion was degassed under reduced pressure at room temperature for approximately 5 min, 3 mL of the dispersion was gently cast onto the center of a liquid substrate (pentadecane; 0.3 mL) [26,27] in a polytetrafluoroethylene (PTFE) watch dish. The dish was subsequently placed in a thermostat drying oven at 60°C overnight. After the nanoparticle-assembled plate (diameter, around 8 mm) was dried, it was placed on an alumina crucible in a horizontal furnace at

room temperature in air. The furnace was then heated from room temperature to 1000°C at a heating rate of 10°C/min and was maintained at 1000°C for 1 h in ambient air. The heater of the furnace was then automatically turned off, and the plate was naturally cooled in the furnace to room temperature.

The surfaces of the samples were observed using an S-4800 SEM operated at 5 kV after the samples were fixed onto an aluminum stub and sputter-coated with Pt–Pd to minimize sample-charging problems. The surface porosity (percentage of pore area in total area) and the grain size were determined from randomly selected SEM photographs with an image analyzing software (Image J; NIH, Bethesda, MD).

The pore-size distributions, open porosities, and specific surface areas were determined from mercury intrusion porosimetry (AutoPore IV 9520; MicromeriticsInstrument Corp.,Norcross, GA) after the samples were dried under vacuum at 60°C for 24 h.

To identify the crystal phases of the samples, powder XRD measurements were performed using an XRD-6100 (Shimadzu Corp., Kyoto, Japan) equipped with a CuKα radiation source after the samples wereground using a mortar and pestle.The weight ratio of β-tricalcium phosphate (β-TCP) and HAp was determined from the peak intensity ratio of β-TCP(0210) and HAp(211) reflections. Before these determinations, XRD patterns of commercially available pure HAp (Kishida Chemical Co., Ltd., Osaka, Japan; used after calcination at 1000°C for 1 h), β-TCP (Wako Pure Chemical Industries, Ltd.) and their mixtures (1/9, 3/7, 5/5, 7/3, and 9/1 weight ratios) were collected; a linear relationship between the weight ratio and peak intensity ratio was confirmed for the preparation of the linear calibration curve.

2.4. Cell adhesion and differentiation

For cell adhesion testing, 5 samples were prepared for each type of nanoporous BCP composition (HAp/β-TCP ratios varied). As control samples, a tissue culture 48-well multiwell plate (Sumitomo Bakelite Co. Ltd., Tokyo, Japan) and dense HAp (porosity, 0%; CELLYARD pellet; HOYA Corp. Tokyo, Japan) were used. MC3T3-E1 mouse preosteoblast cells (Lot No. 10F002; Health Protection Agency Culture Collections, Salisbury, UK) were cultured on each sample (approximately 5.0×10^4 cells/well; 780 cells/mm^2), which was sterilized with ethylene oxide gas at 60˚C, in 500 μL of an α-minimum essential medium (α-MEM; Wako Pure Chemical Industries, Ltd.) supplemented with 10% heat-inactivated fetal bovine serum (FBS; Lonza, Basel, Switzerland), 50-IU/ml penicillin, and 50-μg/ml streptomycin (Lonza) at 37°C for 3 h in a 48-well multiwell plate. Each sample was washed by pipetting with a Dulbecco's phosphate buffered saline (PBS: without Ca and Mg; pH 7.4; Wako Pure Chemical Industries, Ltd.) three times, following which it was placed in an unused well, and the number of cells that adhered on the sample was counted by colorimetry using a microplate reader (SpectraMax M5; Molecular Devices, LLC., Sunnyvale, CA) at 450 nm after staining with a water-soluble tetrazolium salt (Cell Counting Kit-8; Dojindo Laboratories, Kumamoto, Japan). Data resulting from the tests are presented as means ± standard deviations for the mean (N = 5). Statistical comparisons were performed with the Student's *t* test. The level of statistical significance was defined as $p < 0.05$.

For cell differentiation tests, MC3T3-E1 cells (approximately 5.0×10^3 cells/well; 80 cells/mm^2) were cultured on each sample in the α-MEM medium for 3 days. The cells were then incubated in 500 μL of a differentiation medium supplemented with osteoblast-inducer reagents (1 vol.% ascorbic acid, 0.2 vol.%hydrocortisone, and 2 vol.%β-Glycerophosphate;

Takara Bio Inc., Shiga, Japan), and the medium was exchanged twice a week. After 7-, 14- or 21-day incubation, alkaline phosphatase(ALP) staining (TRACP & ALP double-stain Kit; Takara Bio Inc.) was conducted according to the manufacturer's instructions.

3. Results and Discussion

3.1. CDHAp nanoparticles and nanoparticle-assembled CDHAp

Low crystallinity CDHAp nanoparticles were prepared via a wet chemical process with $Ca(NO_3)_2$ and $(NH_4)_2HPO_4$. To obtain small-sized particles, the reaction was conducted at a relatively low temperature (20°C; room temperature) and high pH (12.0) [26]. According to the SEM observations, the CDHAp nanoparticles after centrifugal washing exhibited a spherical morphology with a diameter of 50 nm and polydispersedparticle size distribution [particle size coefficient of variation (Cv), 21%] (see Supplementary Fig. S1). The Ca/P molar ratio of the nanoparticles was 1.61, as determined from an ICP-AES measurement. The aqueous dispersion of the CDHAp nanoparticles (solid content, 2.0 wt.%) was a viscous liquid, which was attributed to the formation of a network structure caused by particle–particle interactions [28] due to their small particle size (i.e., a large number of particles) and zwitterionic-charged HAp surfaces that consisted of Ca^{2+}, PO_4^{3-}, and OH^- ions. The formation of the nanoparticle network structure is likely responsible for the formation of nanosized pores after the particles were dried. Note that adding Ca^{2+} or PO_4^{3-} salts changes the ζ-potential of HAp surfaces [29]. We observed that the addition of Ca^{2+} or PO_4^{3-} salts improved the dispersion stability of the CDHAp nanoparticles after ultrasonic irradiation, and the resulting nanoparticle-assembled CDHAp had a more densely-packed structure with smaller sized nanopores [26].To prepare the nanoparticle-assembled CDHAp

with the same nanoporous structures (and with varied Ca/P ratios) in this study, ultrasonic irradiation of the CDHAp dispersion after adding Ca^{2+} or PO_4^{3-} salts was not performed. As a result, the dispersion state of the Ca- or PO_4-added CDHAp dispersion that was not exposed to ultrasonic irradiation was apparently the same as that of the original dispersion (without additives).

3.2. Composition of nanoporous calcium phosphates

The X-ray diffraction measurements of the sample before heat treatments showed a broad pattern for HAp, and no other calcium phosphate phases were detected (Supplementary Fig. S2). After thermal treatment at 1000°C, several peaks became more distinct (the widths of the peaks became narrower), which indicates an increase in the crystallinity. Whenthermal treatmentwas performed without additives (Ca/P molar ratio, 1.61), an additional crystalline phase of β-TCP was observed (Fig. 1c; see also the open circle in Fig. 2). Experimental evidence [10] indicates that stoichiometric HAp (Ca/P = 1.67, molar ratio) does not decompose at temperatures as high as 1200°C, and that CDHAp (1.50 <Ca/P < 1.67) decomposes at temperatures above 700°C into a mixture of stoichiometric HAp and β-TCP according to the following reaction:

$$Ca_{10-x}(HPO_4)_x(PO_4)_{6-x}(OH)_{2-x} \dashrightarrow (1-x)\,Ca_{10}(PO_4)_6(OH)_2 + 3x\beta\text{-}Ca_3(PO_4)_2 + x\,H_2O \quad \bullet\bullet\bullet(1)$$

The Ca/P molar ratio calculated from the β-TCP content (34.7 wt.%; see the open circle in Fig. 2) after thermal treatment without additives was 1.606, which corresponded to that (Ca/P molar ratio, 1.61) measured from ICP-AES.

The β-TCP content was linearly (predictably) controlled by adjusting the Ca/P ratio of nanoparticle-assembled CDHAp (Fig. 2). That is, the β-TCP content decreased when water soluble $Ca(NO_3)_2$ was added to an aqueous dispersion of low crystallinity CDHAp nanoparticles (Fig. 1b), and phase pure HAp was obtained after thermal treatment at a Ca/P molar ratio of 1.67 (Fig. 1a; see also the closed triangles in Fig. 2). On the other hand, the β-TCP content increased after adding water soluble $(NH_4)_2HPO_4$ to the aqueous dispersion (Fig. 1d), and phase pure β-TCP was obtained by thermal treatment at a Ca/P molar ratio of 1.50 (Fig. 1e; see also the closed squares in Fig. 2). These results support our assumption that the Ca or PO_4 salts were homogeneously distributed in the nanopores of nanoparticle-assembled CDHAp, and they homogeneously reacted with CDHAp.

<Fig. 1>

<Fig. 2>

3.2. Morphologies of nanoporous calcium phosphates

Figure 3 shows SEM photographs of the surfaces of the nanoparticle-assembled CDHAp after thermal treatment. The samples before thermal treatment had small-sized pores (around 8 nm [26]; see also Supplementary Fig. S1), and all the CDHAp prepared with different Ca/P ratios also had nanosized pores on their surfaces before thermal treatment. After thermal treatment at 1000°C, the sizes of the crystal grains measured from SEM images were almost the same (210–300 nm) among the different Ca/P samples (Table 1), but the size tended to increase slightly when theCa/P ratio decreased. The SEM observation also revealed that the surface porosities were also almost the same (18–22%) among the different

Ca/P samples (Table 1), but the porosity tended to decrease when theCa/P ratio decreased. These results suggest that the β-TCP componentslightly promoted the grain growth during thermal treatment. It was shown using selective area electron diffraction (SAED) [30] that TCP grains grew coarser (~0.5 μm) than HAp grains (~0.1 μm) in the case of hot-pressed sintered (1100°C; 20 MPa; 30 min) BCP (88% HAp and 12% β-TCP).

<Fig. 3>

<Table 1>

Mercury intrusion porosimetry was performed to quantitatively determine the pore-size distributions, open porosity, and specific surface areas. Figure 4 shows the pore-size distributions of the samples after thermal treatment withdifferent Ca/P ratios. In the case of the sample without additives (Ca/P molar ratio of 1.61), the pore-size distribution was sharp, and the mean pore size was 173 nm (Table 1). In the cases of samples with $Ca(NO_3)_2$or $(NH_4)_2HPO_4$, the peak top position was almost the same for all samples but an extended tail ofsmaller sizewas observed.The porosities and specific surface areas also decreased after adding both types of additives (Table 1). These results indicate that both $Ca(NO_3)_2$ (1/10, w/w vs. CDHAp) and $(NH_4)_2HPO_4$ (1/20, w/w vs.CDHAp) enhanced densification of BCP during the thermal treatment at 1000°C in ambient air.Because $Ca(NO_3)_2$ melts at 561°C [31], the liquid phase might promote densification via liquid phase sintering [32,33]. The surface morphology (grain size and surface porosity) was not significantly different between the samples,as described above, which might be due to the preferential decomposition of $Ca(NO_3)_2$ (around 680°C [31]) into CaO (melting point, 2850 ℃)on the sample

surfaces.Sodium phosphate (Na_3PO_4) has been reported be an effective additive for enhancing sintering (densification) of HAp but the additive does not seem to affect grain growth strongly [34]. Note that that the improved sinterabilitywhen adding $Na_3PO_4$is also attributed to the formation of OH vacancies in the Na-substituted HAp, butsodium salts were not used in this study.

<Fig. 4>

3.3. Cell adhesion and differentiation on nanoporous calcium phosphates

Initial cell adhesion tests on composition-controlled nanoporouscalcium phosphateswith similar surface morphologieswere conducted with MC3T3-E1 mouse preosteoblast cells cultured for 3 h (Figs. 5 and 6). In this study,a commercially available dense HAp and a tissue culture plate were used as control samples. The cell differentiation was also evaluated with ALP staining afterculturing MC3T3-E1 cells on each sample in a differentiation medium (Fig. 7).

The nanoporous HAp showed statistically significant improvement ininitial cell adhesion compared with dense HAp (Fig. 5).Fromthe morphological observation with the SEM, the cells that adhered to the nanoporous HAp (Fig. 6b) elongated with a fusiform fibroblastic appearance as compared with the dense HAp (Fig. 6a). These results support that osteoblastic cells adhesion was affected by not only the chemistry of HAp but also the surface topography, such as the degree of roughness and microdomain structure, as has been previously observed [35–39].Cell adhesion, proliferation, and detachment strength were sensitive to surfaceroughness and,these parameters increased with increasing HAp

roughness [38]; also, the structure and size of the phase-separated microdomains on the block copolymer, the blocks of which had different protein adhesion properties, influenced the cell adhesion due to the “capping control” of the membrane proteins on the cells [39].

<Fig. 5>

<Fig. 6>

Next, we compared the three types of nanoporous calcium phosphates. Although no significant differenceswere observed in initial cell adhesion among the nanoporous samples (Fig. 5), the cells on thenanoporous BCP (β-TCP, 35 wt.%)orpure β-TCP surfaces had expanded cytoskeletonsthat were spread out (Figs. 6c and 6d), which wasin contrast to the elongated cells that exhibited fusiform fibroblastic appearance on nanoporous pure HAp (Fig. 6b).ALP staining revealed that cell differentiation was promoted on the nanoporous HAp compared with the nanoporous BCP and β-TCP.Previous in vitro work with MC3T3-E1 cells has shown that elevated levels of both extracellular Ca and PO_4 ions decrease cell viability [40–42].Suzuki *et al.* reported that the PO_4 concentration was increased in an Eagle’s minimum essential medium that was supplemented with 10% FBS by decreasing the Ca/P ratio of the BCP while the Caconcentration remained constant [43], and this might be the reason why cell differentiation on nanoporous BCP or β-TCP was suppressed compared with nanoporous HAp.

<Fig. 7>

The BCP composition influences the degradation rate and the osteogenic potency in vivo. Habibovic *et al.* obtained significantly more boneformationingoats by implanting BCP with a HAp/β-TCP ratio of 88/12 as compared to pure HAp, attributing the lower bone formation to the limited degradation rate [44].Arinzeh *et al.*prepared BCP from a mixture of pure HAp and pure β-TCP, and human mesenchymal stem cell (hMSC) bone induction occurred at the fastest rate in vivo compared to the other 100%-HAp formulations, including HAp/β-TCP (76/24, 63/37, 56/44) and 100% TCP [45]. As reported by Kurashina *et al.*, bone formation was onlydetected after implantation of porous BCP with anHA/β-TCP ratio of70/30 [46].The aforementionedresultselucidatethatit is not only the chemical composition that plays a critical role in bone tissue engineering but parameters such as microstructure [47,48], specific surface area [44,49],and macrostructure [50], as well as host anatomy and physiology,also are important [49].The in vivo evaluation of the nanoporous calcium phosphates prepared here is now being attempted, and the in vivo influence of the BCP composition with similar surface morphologieswill be clarified in the near future.

4. Conclusion

In this study, we aimed to develop a simple colloidal process for preparingnanoporousBCP with well-controlled HAp/β-TCP ratios and approximately the same surface morphologies (grain size, surface pore size, and surface porosity). This process consists of (1) the preparation of an aqueous dispersion of low-crystallinity CDHAp nanoparticles used as the building block, (2) the adjustment of the Ca/P molar ratio by dissolving Ca or PO_4 salts in the aqueous dispersion, (3) the preparation of the nanoparticle-assembled plates by drying the nanoparticle dispersion, and (4) the preparation

of nanoporous BCP by thermal treatment.This process requires no pore generation agents such as surfactant micelle templates and porogens, and the composition of BCP could be easily and predictably controlled by adjusting of the Ca/P molar ratio.Although we prepared nanoporous BCPs in a plate form in this study, this process is also applicable to control the compositions and surface morphologies of BCP in granule and macroporous forms prepared via colloidal processes, such as spray drying and the polymer sponge method. The nanoporousBCP ceramics developed in this study have potential applications in orthopedics, dentistry, and tissue engineering. Our final goal is to develop a novel artificial bone graft for alveolar cleft in children with cleft lip or cleft lip and palate.Although this study focused on calcium phosphates, this approach can help in the fabrication of mesoporous (or nanoporous) materials with other low-crystallinity fine ceramics for use as ceramic catalysts and photonic bandgap crystals.

Acknowledgments

The SEM observations, XRD measurements and in vitro tests were performed at the Institute of Dental Research, Osaka Dental University. This study was supported in part by JSPS KAKENHI Grant Number 23792301, and by a grant program of the Feasibility Study Stage in Adaptable and Seamless Technology Transfer Program through Target-driven R&D (A-STEP; ID: AS231Z01647C) from Japan Science and Technology Agency (JST).

Supplementary material

The online version of this article contains additional supplementary material.

REFERENCES

[1] S.V. Dorozhkin, ActaBiomater. Biphasic, triphasic and multiphasic calcium orthophosphates, 8 (2012) 963–977.

[2] S. Bose, S. Tarafder, Calcium phosphate ceramic systems in growth factor and drug delivery for bone tissue engineering: A review, ActaBiomater. 8 (2012) 1401–1421.

[3] G. Daculsi, S. Baroth, R.Z. LeGeros, 20 years of biphasic calcium phosphate bioceramics development and applications, in: R. Narayan, P. Colombo, D. Singh, J. Salem (Eds.), Advance in bioceramics and porous ceramics II, Wiley-American Ceramic Society, Newyork, 2010, pp. 45–58.

[4] M. Jarcho, Calcium phosphate ceramics as hard tissue prosthetics. Clin. Orthop. Relat. Res. 157 (1981) 259–278.

[5] R.F. Ellinger, E.B. Nery, K.L. Lynch, Histological assessment of periodontal osseous defects following implantation of hydroxyapatite and biphasic calcium phosphate ceramics: a case report, Int. J. Periodont. Restor. Dent. 3 (1986) 223–233.

[6] E.B.Nery, K.K. Lee, S. Czajkowski, J.J. Dooner, M. Duggan, R.F. Ellinger, J.M. Henskin, R. Hines, M. Miller, J.W. Olson, M. Rafferty, T. Sullivan, P. Walters, D. Welch, A. Williams,A Veterans Administration Cooperative Study of biphasic calcium phosphate ceramic in periodontal osseous defects, J. Periodontol. 61 (1990) 737–744.

[7] G. Daculsi, R.Z. Legeros, E. Nery, K. Lynch, B. Kerebel, Transformation of biphasic calcium phosphate ceramics *in vivo*: Ultrastructural and physicochemical characterization, J. Biomed. Mater. Res. 23 (1989) 883–894.

[8] E.B. Nery, R.Z. LeGeros, K.L. Lynch, K. Lee, Tissue response to biphasic calcium phosphate ceramic with different ratios of HA/beta TCP in periodontal osseous defects,J.

Periodontol. 63 (1992) 729–735.

[9] R.Z. LeGeros, S. Lin, R. Rohanizadeh, D. Mijares, J.P. LeGeros, Biphasic calcium phosphate bioceramics: preparation, properties and applications, J. Mater. Sci. Mater. Med. 14 (2003) 201–209.

[10] S. Raynaud, E. Champion, D. Bernache-Assollant, P. Thomas, Calcium phosphate apatites with variable Ca/P atomic ratio I. Synthesis, characterisation and thermal stability of powders, Biomaterials 23 (2002) 1065–1072.

[11] A.K. Guha, S. Singh, R. Kumaresan, S. Nayar, A. Sinha, Mesenchymal cell response to nanosized biphasic calcium phosphate composites, Colloids Surf. B Biointerfaces73 (2009) 146–151.

[12] M. Okada, T. Furuzono, Hydroxylapatite nanoparticles: fabrication methods and medical applications, Sci. Technol. Adv. Mater. 13 (2012) 064103.

[13] M. Descamps, L. Boilet, G. Moreau, A. Tricoteaux, J. Lu, A. Leriche, V. Lardot, F. Cambier, Processing and properties of biphasic calcium phosphates bioceramics obtained by pressureless sintering and hot isostatic pressing, J. Eur. Ceram. Soc. 33 (2013) 1263–1270.

[14] X. Yang, Z. Wang, Synthesis of biphasic ceramics of hydroxyapatite and β-tricalcium phosphate with controlled phase content and porosity, J. Mater. Chem. 8 (1998) 2233–2237.

[15] T.R. Tadjiev, C. Sungsu, K. Sukyoung, Mechano-Chemical Synthesis of Biphasic Calcium Phosphates with the Various Ratio of HA and β-TCP, Key Eng. Mater. 330–332 (2007) 7–10.

[16] R.R. Rao, H.N. Roopa, T.S. Kannan, Solid state synthesis and thermal stability of HAP

and HAP – β-TCP composite ceramic powders, J. Mater. Sci. Mater. Med. 8 (1997) 511–518.

[17] C.-K. Hsu, The preparation of biphasic porous calcium phosphate by the mixture of $Ca(H_2PO_4)_2 \cdot H_2O$ and $CaCO_3$, Mater. Chem. Phys. 80 (2003) 409–420.

[18] K.S. Jaw, Preparation of a biphasic calcium phosphate from $Ca(H_2PO_4)_2 \cdot H_2O$ and $CaCO_3$, J. Therm. Anal. Calorim. 83 (2006) 145–149.

[19] M. Ebrahimi, P. Pripatnanont, N. Monmaturapoj, S. Suttapreyasri, Fabrication and characterization of novel nano hydroxyapatite/β-tricalcium phosphate scaffolds in three different composition ratios, J. Biomed. Mater. Res. A 100 (2012) 2260-2268.

[20] S. Impens, R. Schelstraete, J. Luyten, S. Mullens, I. Thijs, J. van Humbeeck, J. Schrooten, Production and characterisation of porous calcium phosphate structures with controllable hydroxyapatite/β-tricalcium phosphate ratios, Adv. Appl. Ceram. 108 (2009) 494–500.

[21] T. J. Webster, C. Ergun, R. H. Doremus, R. W. Siegel, R. Bizios, Enhanced osteoclast-like cell functions on nanophase ceramics, Biomaterials 22 (2001) 1327–1333.

[22] G. Balasundaram, M. Sato, T. J. Webster, Using hydroxyapatite nanoparticles and decreased crystallinity to promote osteoblast adhesion similar to functionalizing with RGD, Biomaterials 27 (2006) 2798–2805.

[23] W. Sun, C. Chu, J. Wang, H. Zhao, Comparison of periodontal ligament cells responses to dense and nanophase hydroxyapatite, J. Mater. Sci. Mater. Med. 18 (2007) 677–683.

[24] J. Huang, S. M. Best, W. Bonfield, R. A. Brooks, N. Rushton, S. N. Jayasinghe, M. J. Edirisinghe, In vitro assessment of the biological response to nano-sized hydroxyapatite,

J. Mater. Sci. Mater. Med. 15 (2004) 441–445.

[25] M.R. Appleford, S. Oh, N. Oh, J.L. Ong, In vivo study on hydroxyapatite scaffolds with trabecular architecture for bone repair, J. Biomed. Mater. Res. A 89 (2009) 1019–1027.

[26] M. Okada, T. Furuzono, Low-temperature synthesis of nanoparticle-assembled, transparent, and low-crystallized hydroxyapatite blocks, J. Colloid Interface Sci. 360 (2011) 457–462.

[27] M. Okada, K. Fujiwara, M. Uehira, N. Matsumoto, S. Takeda, Expansion of nanosized pores in low-crystallinity nanoparticle-assembled plates via a thermally induced increase in solid-state density, J. Colloid Interface Sci. 405 (2013) 58–63.

[28] Ir. R. Rutgers, Relative Viscosity and Concentration, Rheol. Acta. 2 (1962) 305–348.

[29] P. Somasundaran, Y. H. C. Wang, Surface chemical characteristics and adsorption properties of apatite.in: D. N. Misra (Ed.), Adsorption on and Surface Chemistry of Hydroxyapatite, Plenum Press, New York, 1984, pp. 129-149.

[30] E. Champion, Sintering of calcium phosphate bioceramics, ActaBiomater. 9 (2013) 5855–5875.

[31] C. Ettarh, A.K. Galwey, A kinetic and mechanistic study of the thermal decomposition of calcium nitrate, Thermochim. Acta, 288 (1996) 203–219.

[32] W.D. Kingery, Densification during Sintering in the Presence of a Liquid Phase. I. Theory, J. Appl. Phys. 30 (1959) 301–306.

[33] J.E. Marion, C.H. Hsueh, A.G. Evans, Liquid Phase Sintering of Ceramics, J. Am. Ceram. Soc. 70 (1987) 708–713.

[34] L.V. Fateeva, Y.I. Golovkov, S.V. Tumanov, S.M. Barinov, A.N. Shemyakina, V.P. Orlovskii, F. Rustikelli, S. Oskarsson, Effect of Sodium Phosphate on Sintering of

Hydroxyapatite Ceramics, Refract. Ind. Ceram. 42 (2001) 3–8.

[35] K. Anselme, M. Bigerelle, B. Noel, E. Dufresne, D. Judas, A. Iost, P. Hardouin, Qualitative and quantitative study of human osteoblast adhesion on materials with various surface roughnesses, J. Biomed. Mater. Res. 49 (2000) 155–166.

[36] K. Anselme, M. Bigerelle, Topography effects of pure titanium substrates on human osteoblast long-term adhesion, ActaBiomater. 1 (2005) 211–222.

[37] N. Ribeiro, S.R. Sousa, F.J. Monteiro, Influence of crystallite size of nanophased hydroxyapatite on fibronectin and osteonectin adsorption and on MC3T3-E1 osteoblast adhesion and morphology, J. Colloid Interface Sci. 351 (2010) 398–406.

[38] D.D. Deligianni, N.D. Katsala, P.G. Koutsoukos, Y.F. Missirlis, E!ect of surface roughness of hydroxyapatite on human bone marrow cell adhesion, proliferation, di!erentiation and detachment strength, Biomaterials 22 (2001) 87–96.

[39] T. Okano, M. Uruno, N. Sugiyama, M. Shimada, I. Shinohara, K. Kataoka, Y. Sakurai, Suppression of platelet activity on microdomain surfaces of 2-hydroxyethyl methacrylate-polyether block copolymers, J. Biomed. Mater. Res. 20 (1986) 1035–1047.

[40] Z. Meleti, I.M. Shapiro, C.S. Adams, Inorganic Phosphate Induces Apoptosis of Osteoblast-like Cells in Culture, Bone 27 (2000) 359–366.

[41] C.S. Adams, K. Mansfield, R.L. Perlot, I.M. Shapiro,Matrix Regulation of Skeletal Cell Apoptosis. Role of calcium and phosphate ions, J. Biol. Chem. 276 (2001) 20316–20322.

[42] E.J. Tsang, C.K. Arakawa, P.A. Zuk, B.M. Wu, Osteoblast Interactions Within a Biomimetic Apatite Microenvironment, Ann. Biomed. Eng. 39 (2011) 1186–1200.

[43] T. Suzuki, T. Yamamoto, M. Toriyama, K. Nishizawa, Y. Yokogawa, M.R. Mucalo, Y. Kawamoto, F. Nagata, T. Kameyama, Surface instability of calcium phosphate ceramics in tissue culture medium and the effect on adhesion and growth of anchorage-dependent animal cells, J. Biomed. Mater. Res. 34 (1997) 507–517.

[44] P. Habibovic, H. Yuan, C. M. van der Valk, G. Meijer, C. A. van Blitterswijk, K. de Groot, 3D microenvironment as essential element for osteoinduction by biomaterials, Biomaterials 26 (2005) 3565–3575.

[45] T.L. Arinzeh, T. Tran, J. Mcalary, G. Daculsi, A comparative study of biphasic calcium phosphate ceramics for human mesenchymal stem-cell-induced bone formation, Biomaterials 26 (2005) 3631–3638.

[46] K. Kurashina, H. Kurita, Q. Wu, A. Ohtsuka, H. Kobayashi, Ectopic osteogenesis with biphasic ceramics of hydroxyapatite and tricalcium phosphate in rabbits, Biomaterials 23 (2002) 407–412.

[47] K.A. Hing, B. Annaz, S. Saeed, P.A. Revell, T. Buckland, Microporosity enhances bioactivity of synthetic bone graft substitutes, J. Mater. Sci. Mater. Mad. 6 (2005) 467–475.

[48] D. Le Nihouannen, G. Daculsi, A. Saffarzadeh, O. Gauthier, S. Delplace, P. Pilet, P. Layrolle, Ectopic bone formation by microporous calcium phosphate ceramic particles in sheep muscles, Bone 36 (2005) 1086–1093.

[49] B. H. Fellah, O. Gauthier, P. Weiss, D. Chappard, P. Layrolle, Osteogenicity of biphasic calcium phosphate ceramics and bone autograft in a goat model, Biomaterials 29 (2008) 1177–1188.

[50] M. Mastrogiacomo, S. Scaglione, R. Martinetti, L. Dolcini, F. Beltrame, R. Cancedda, R.

Quarto, Role of scaffold internal structure on in vivo bone formation in macroporous calcium phosphate bioceramics, Biomaterials 27 (2006) 3230–3237.

Table 1. Characterizations of nanoporous calcium phosphates

	Grain size[d] (nm)	Surface porosity[e] (%)	Mean poresize[f] (nm)	Open porosity[f] (%)	Specific surfacearea[f] (m^2/g)
HAp[a]	210 ± 60	21.9 ± 0.6	157	20	2.3
BCP[b]	229 ± 67	19.3 ± 1.1	173	53	8.4
β-TCP[c]	304 ± 105	17.9 ± 1.0	143	14	1.8

[a] Prepared with $Ca(NO_3)_2$ (Ca/P=1.66, molar ratio)

[b] Prepared without additives (β-TCP content, 35 wt.%)

[c] Prepared with $(NH_4)_2HPO_4$ (Ca/P=1.50, molar ratio)

[d] Percentage of pore region area in total area, measured from SEM images (N = 50)

[e] Measured from SEM images (N =3)

[f] Measured with a mercury intrusion porosimetry

FIGURE CAPTIONS

Figure 1. XRD patterns of nanoparticle-assembled CDHAp after thermal treatment at 1000°C. The CDHAp were prepared by drying CDHAp dispersions with added $Ca(NO_3)_2$ or $(NH_4)_2HPO_4$ to adjust Ca/P molar ratios: (a) 1.67, (b) 1.64, (c) 1.61 (without additives), (d) 1.56,and (e) 1.50.

Figure 2. β-TCP contents in nanoparticle-assembled CDHAp with different Ca/P ratios after thermal treatment at 1000°C. The CDHAp were prepared (○) without and with additives: ▲, $Ca(NO_3)_2$; ■, $(NH_4)_2HPO_4$

Figure 3. SEM photographs of nanoparticle-assembled CDHAp after thermal treatment at 1000°C. The CDHAp were prepared by drying CDHAp dispersions with added $Ca(NO_3)_2$ and $(NH_4)_2HPO_4$ to adjust the Ca/P molar ratios: (a) 1.67, (b) 1.61 (without additives), and (c) 1.50.

Figure 4. Pore size distributions of nanoparticle-assembled CDHAp after thermal treatment at 1000°C. The CDHAp were prepared by drying CDHAp dispersions with added $Ca(NO_3)_2$ and $(NH_4)_2HPO_4$ to adjust Ca/P molar ratios: (a) 1.67, (b) 1.61 (without additives), and (c) 1.50.

Figure 5. Initial MC3T3-E1 cell adhesion after 3-h incubation on (a) dense HAp, (b) nanoporous HAp, (c) nanoporous BCP (β-TCP, 35 wt.%), (d) nanoporousβ-TCP, and (e) tissue culture plate. Initial cell density was 780 cells/mm^2.

Figure 6. SEM photographs of MC3T3-E1 cells after 3-h incubation on (a) dense HAp, (b) nanoporous HAp, (c) nanoporous BCP (β-TCP, 35 wt.%), (d) nanoporousβ-TCP, and (e) tissue culture plate. The photographs (a')–(e') show magnified images.

Figure 7. Alkaline phosphatase staining of cells incubated on the samples in differentiation media.

Figure(s)

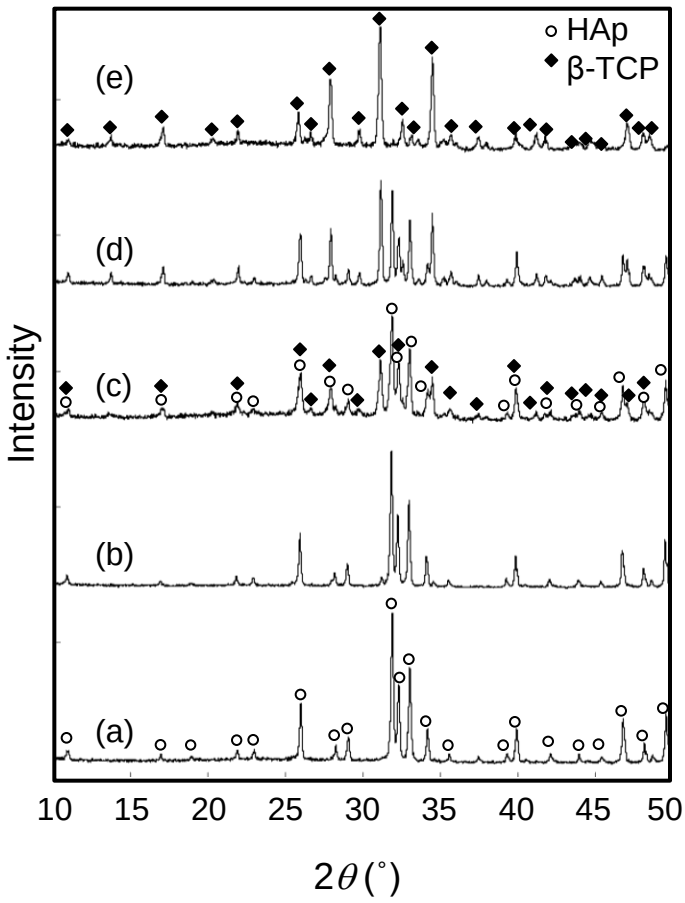

Figure 1. XRD patterns of nanoparticle-assembled CDHAp after thermal treatment at 1000° C. The CDHAp were prepared by drying CDHAp dispersions with added $Ca(NO_3)_2$ or $(NH_4)_2HPO_4$ to adjust Ca/P molar ratios: (a) 1.67, (b) 1.64, (c) 1.61 (without additives), (d) 1.56, and (e) 1.50.

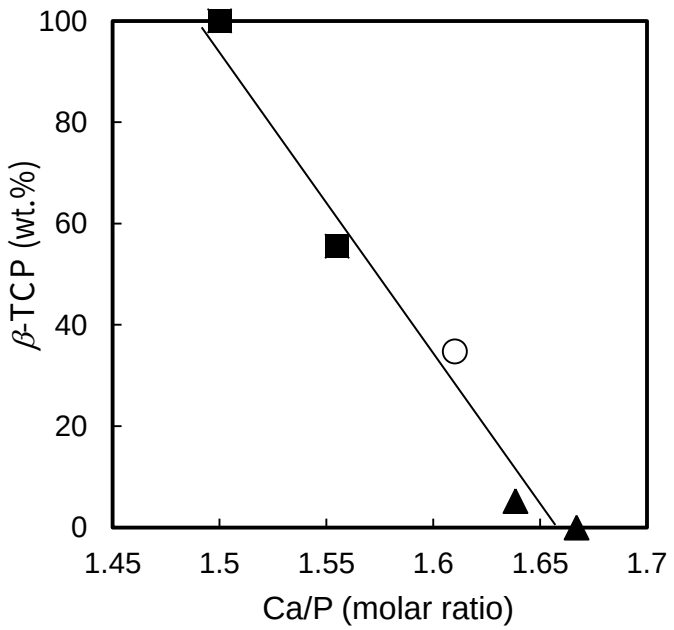

Figure 2. β-TCP contents in nanoparticle-assembled CDHAp with different Ca/P ratios after thermal treatment at 1000° C. The CDHAp were prepared (○) without and with additives: ▲, $Ca(NO_3)_2$; ■, $(NH_4)_2HPO_4$

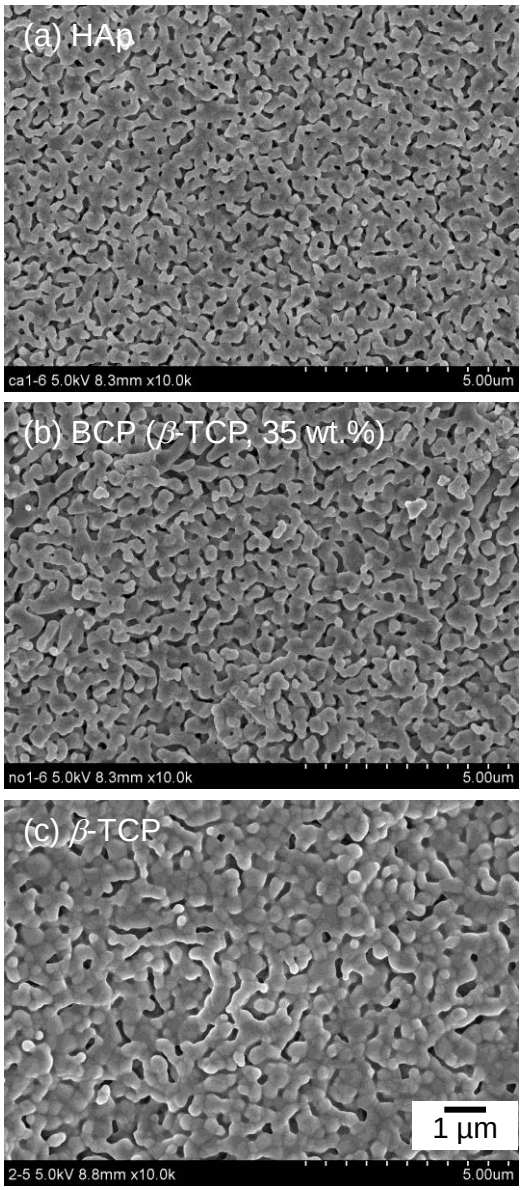

Figure 3. SEM photographs of nanoparticle-assembled CDHAp after thermal treatment at 1000° C. The CDHAp were prepared by drying CDHAp dispersions with added $Ca(NO_3)_2$ and $(NH_4)_2HPO_4$ to adjust the Ca/P molar ratios: (a) 1.67, (b) 1.61 (without additives), and (c) 1.50.

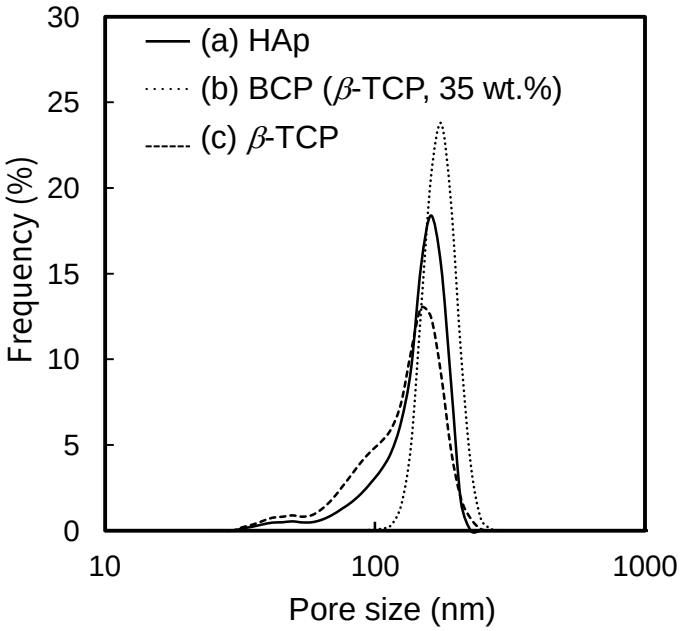

Figure 4. Pore size distributions of nanoparticle-assembled CDHAp after thermal treatment at 1000° C. The CDHAp were prepared by drying CDHAp dispersions with added Ca(NO3)2 and (NH4)2HPO4 to adjust Ca/P molar ratios: (a) 1.67, (b) 1.61 (without additives), and (c) 1.50.

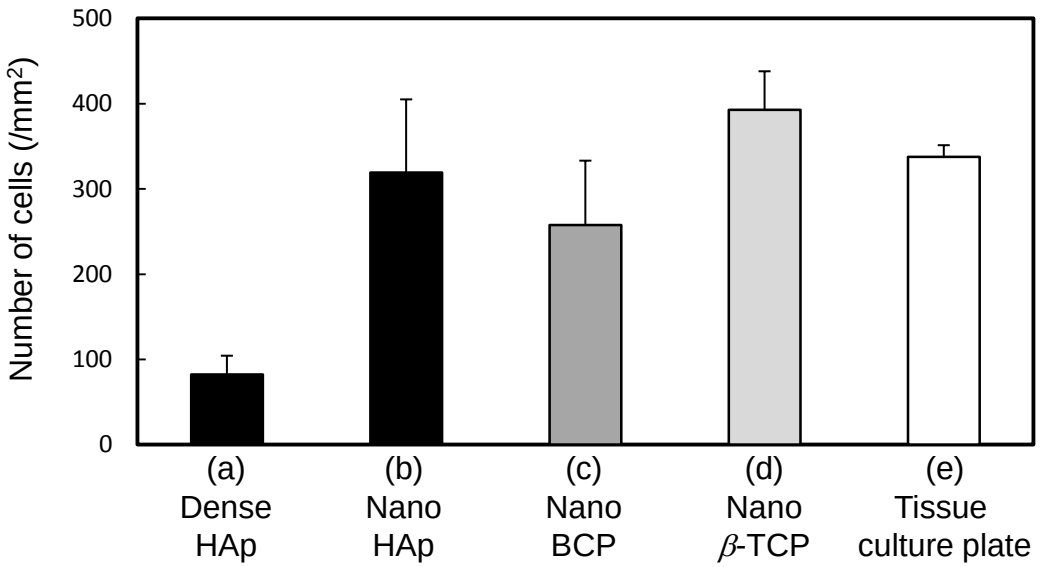

Figure 5. Initial MC3T3-E1 cell adhesion after 3-h incubation on (a) dense HAp, (b) nanoporous HAp, (c) nanoporous BCP (β-TCP, 35 wt.%), (d) nanoporous β-TCP, and (e) tissue culture plate. Initial cell density was 780 cells/mm^2.

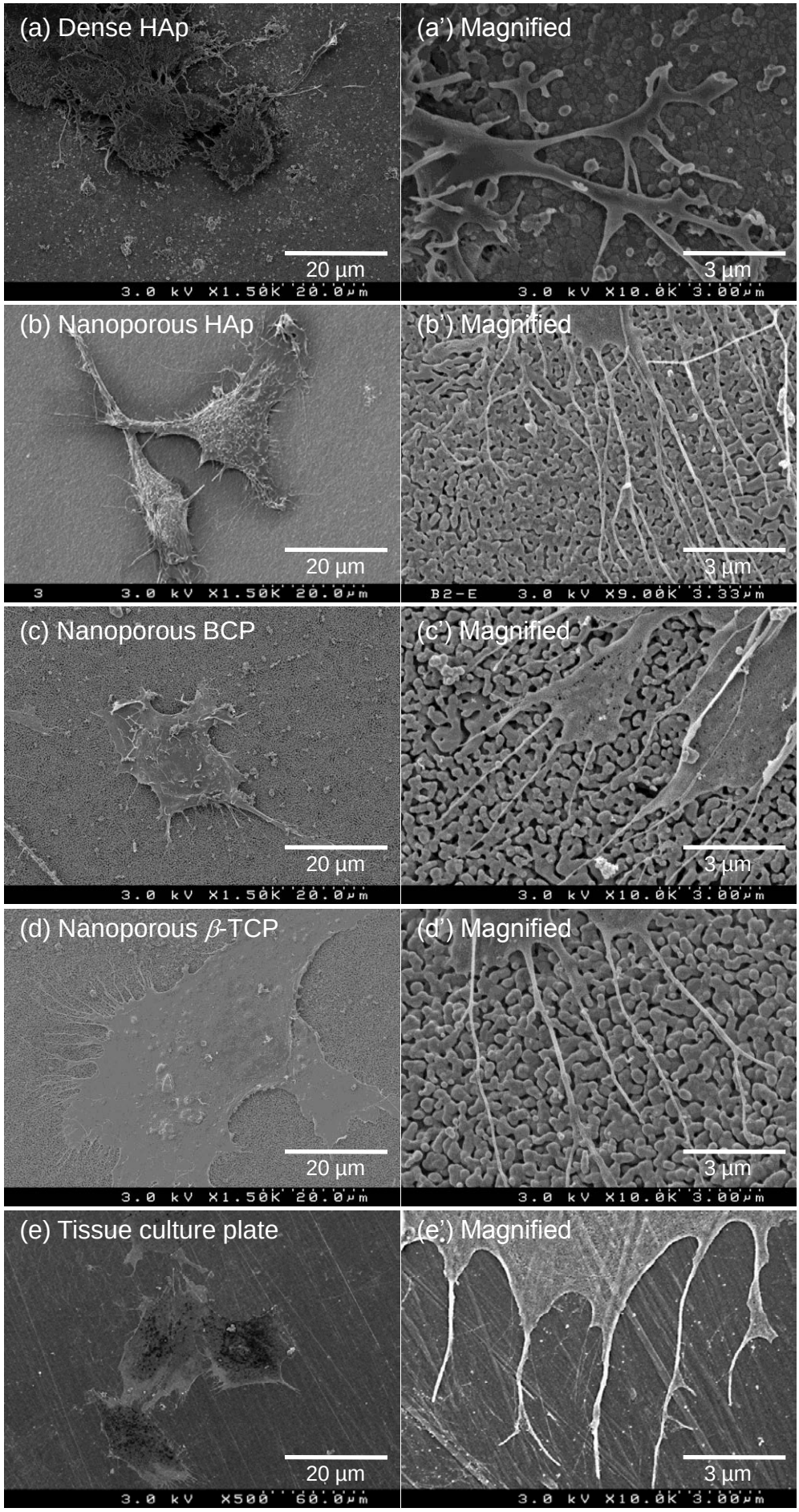

Figure 6. SEM photographs of MC3T3-E1 cells after 3-h incubation on (a) dense HAp, (b) nanoporous HAp, (c) nanoporous BCP (β-TCP, 35 wt.%), (d) nanoporous β-TCP, and (e) tissue culture plate. The photographs (a')–(e') show magnified images.

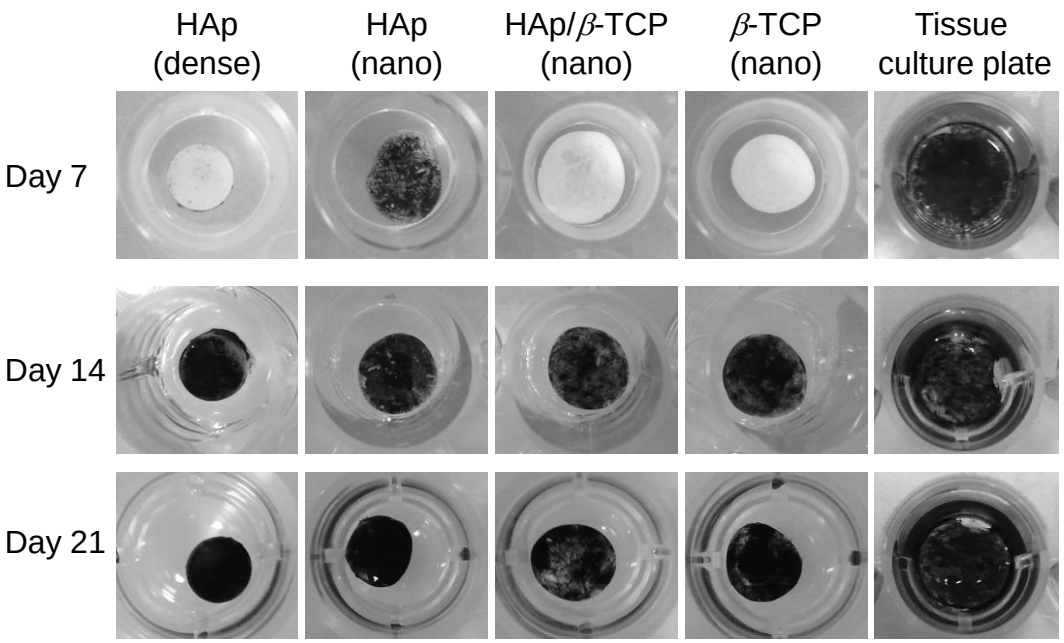

Figure 7. Alkaline phosphatase staining of cells incubated on the samples in differentiation media.